Environmental Science & Technology

Article

Cite This: Environ. Sci. Technol. 2019, 53, 6094−6102

pubs.acs.org/est

Reducing Energy Penalty of CO_2 Capture Using Fe Promoted SO_4^{2-}/ZrO_2/MCM-41 Catalyst

Xiaowen Zhang, Zhiqing Zhu, Xiaoyu Sun, Jian Yang, Hongxia Gao,* Yangqiang Huang, Xiao Luo, Zhiwu Liang,* and Paitoon Tontiwachwuthikul

Joint International Center for CO_2 Capture and Storage (iCCS), Provincial Hunan Key Laboratory for Cost-effective Utilization of Fossil Fuel Aimed at Reducing CO_2 Emissions, College of Chemistry and Chemical Engineering, Hunan University, Changsha 410082, PR China

Supporting Information

ABSTRACT: The high energy consumption of CO_2-loaded solvent regeneration is the biggest impediment for the real application of the amine-based CO_2 capture process. To lower the energy requirement, three Fe promoted SO_4^{2-}/ZrO_2 supported on MCM-41 (SZMF) catalysts with different iron oxide content (5%, 10%, and 15%) were synthesized and applied for the rich monoethanolamine solution regeneration process at 98 °C. Results reveal that the use of SZMF hugely enhanced the CO_2 desorption performances (i.e., desorption factor) by 260−388% and reduced the heat duty by about 28−40%, which is better than most of the reported catalysts for this purpose. The eminent catalytic activities of SZMF are related to their enhanced ratio of Brønsted to Lewis acid sites, weak acid sites, basic sites, and high dispersed Fe^{3+} species. Meanwhile, the addition of SZMF for CO_2 desorption shows a promotional effect on its CO_2 absorption performance, and SZMF presents an excellent cyclic stability. A possible mechanism is suggested for the SZMF catalyzed CO_2 desorption process. Results of this work may provide direction for future research and rational design of more efficient catalysts for this potential catalyst-aided CO_2 desorption technology.

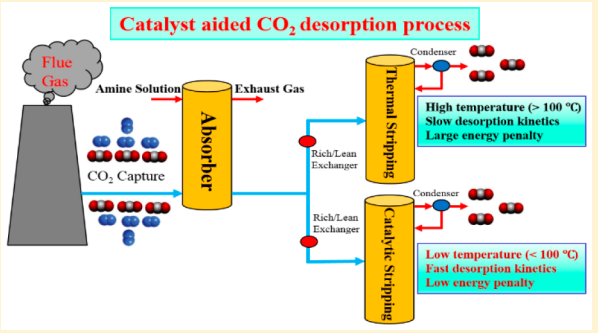

1. INTRODUCTION

Owing to the extensive use of fossil fuel in modern industries, a quantity of carbon dioxide (CO_2) is discharged to the atmosphere, resulting in many environmental issues, such as the abominable greenhouse effect.[1−5] At the moment, one of the most economical and effective techniques for postcombustion CO_2 capture is the amine-based solution absorption method.[6−9] Aqueous monoethanolamine (MEA) (5 M, 30 wt %) solution has been considered as the benchmark for this method.[10−12] However, the amine solvent absorption method requires a large amount of heat duties for CO_2 desorption, which contributes to more than 50% of the operation costs in a CO_2 capture unit.[13−17] The heat duty associated with the rich amine solvent regeneration remains the most critical challenge for the large-scale implementation of this method for CO_2 capture.[18−20] Despite considerable efforts to decrease energy consumption of regeneration, including modifying process configurations and using new amine formulation, advanced technology of overcoming this obstacle is still strong demanded.[21−23]

Recently, an innovative approach for greatly reducing heat duty of amine solvent regeneration was proposed in our earlier works.[24,25] The use of acid catalysts for the CO_2 desorption process mainly decreases the sensible heat and evaporation heat by donating the proton to aid the breakdown of carbamate and lowering the desorption temperature from 120 to 140 °C to a temperature less than 100 °C.[25,26] The results demonstrated that the introduction of the solid acid catalysts into the rich amine solvent could significantly reduce the energy requirement. Various solid catalysts, such as zeolites, metal oxides, sulfated metal oxides, carbonic anhydrase, and metal modified zeolites, have been evaluated for this objective.[10,18,24,27−34] A brief review of investigations for the catalytic rich MEA solution regeneration process over solid acid catalysts is summarized in Table S3. Note that compared with the catalyst-free run, the addition of the different solid acid catalysts with 5 M MEA lowered the energy consumption by approximately 10−34% and increased the quality of released CO_2 by approximately 10−94%, respectively. However, the introduction of solid acid catalysts to increase the CO_2 desorption kinetics is in its infant stages and has not yet obtained commercial application.

Previous work implied that a catalyst synchronously has the high Brønsted acid sites (BAS) and Lewis acid sites (LAS), and a large mesoporous surface area (MSA) would bring forth superior catalytic desorption activity for the amine solvent regeneration process.[24,26,35] Shi et al.[25] revealed that the basic group HCO_3^- could act as a "catalyst" to facilitate the

Received: March 29, 2019
Accepted: April 22, 2019
Published: April 22, 2019

DOI: 10.1021/acs.est.9b01901
Environ. Sci. Technol. 2019, 53, 6094−6102

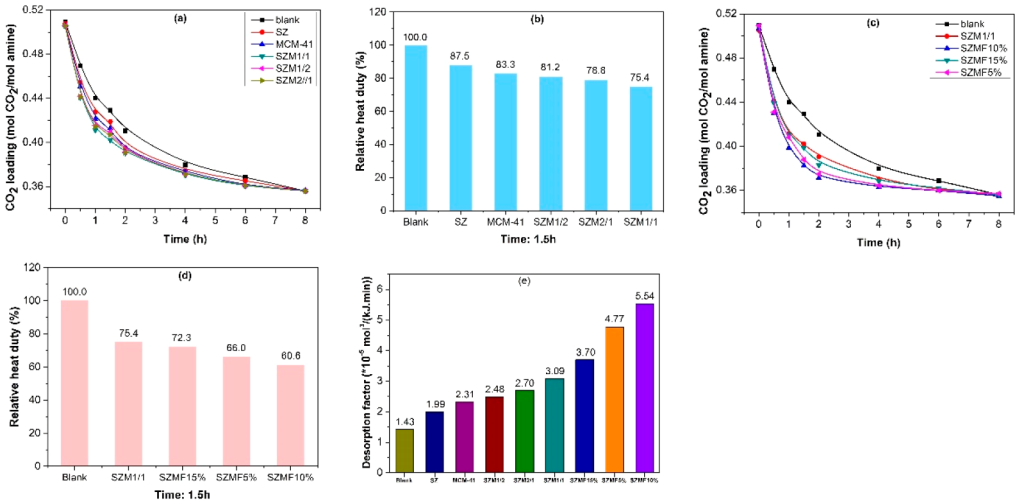

Figure 1. Catalytic CO_2 desorption performance in 5 M MEA solution with different catalysts at 60−98 °C. The weight ratio of the catalyst with MEA solution is 1.25%: (a) CO_2 loading change curves with the SZM catalysts, (b) relative heat duty of MEA with the SZM catalysts, (c) CO_2 loading change curves with the SZMF catalysts, (d) relative heat duty of MEA with the SZMF catalysts, and (e) desorption factor of all the cases.

deprotonation reaction for the CO_2 desorption process. Hence, there is a desirable chance to further enhance the catalytic CO_2 desorption activity by obtaining the more efficient catalysts with the multifold favorable characters. Also, the concept of catalyst-aided amine solvent regeneration is new and limited to only a few catalysts, and plenty of studies are still demanded in this field to find better catalysts and evaluate their techno-economic feasibility.

Sulfated zirconia (SO_4^{2-}/ZrO_2, SZ), a subfamily of solid acid catalysts, has been adopted in the rich amine regeneration reaction due to its vigorous acidity.[27,36] However, the relatively small surface, the nonuniform pore size, and the rapid deactivation of SZ restrict its use in catalyzing the CO_2 desorption process.[37] Mesoporous material MCM-41 possesses attractive catalytic features including large specific area, uniform-sized pores, and small diffusion hindrance.[38−41] The introduction of SZ and MCM-41 into the 5 M rich MEA solution for CO_2 desorption could reduce the heat duty by about 10% and 20% compared with the blank run.[27] Nevertheless, the acid strength of the pure silicon MCM-41 is relatively weak, which hinders its catalysis applications.[42] As a result, the use of MCM-41 as a catalyst support for SZ might greatly enlarge the catalytic capabilities of SZ for catalyzing the CO_2 desorption process. This is because of such a composite catalyst SZ supported on MCM-41 (SZM), which would simultaneously possess the high BAS and LAS, relatively large MSA, and high stability.[24,43] These properties will surely facilitate the CO_2 desorption in a rich amine solution.

For another, the metal-zeolite hybrid catalysts, i.e., Fe/MCM-41 and Fe/ZSM-5, have been extensively studied for many chemical reactions, due to the fact that the doping iron oxide into the MCM-41 has been proved to increase the acidity and basicity.[44−46] Also, Fe_2O_3 is nontoxic, low cost, abundant, and environmentally friendly.[47,48] Accordingly, Fe_2O_3 is intentionally selected as the active metal center and is introduced to the SZM to further improve its catalytic properties (e.g., basic and acid sites). It is therefore of great interest to apply the Fe promoted SO_4^{2-}/ZrO_2/MCM-41 (SZMF) catalyst for the rich amine solution regeneration process to further enhance the CO_2 desorption activity and make the CO_2 capture process more economically feasible. To the authors' knowledge, the application of SZMF in the CO_2 desorption process has not been reported heretofore. Furthermore, it is very essential to study the impact of the Fe_2O_3 loading on its catalytic performance, which properties of the catalyst have the greatest influence on the catalytic performance, the stability of catalyst, and the effect of catalyst on the CO_2 absorption behavior.

Herein, a series of Fe promoted SZ supported on MCM-41 catalysts (SZMF) were prepared and applied to improve the regeneration performance of the rich 5 M MEA solvent regeneration process at 98 °C. The catalysts were characterized by various methods. Moreover, the stability of the SZMF and the influence on the SZMF for the CO_2 absorption behavior were studied. The catalytic amine solvent regeneration mechanism over the SZMF catalyst was suggested, and the relationship between catalytic properties and the catalytic performances was explored. The results of our work will suggest some new ideas in advance of the CO_2 capture.

2. MATERIALS AND METHODS

2.1. Materials. The chemicals used in this work are listed in Supporting Information (SI) Section 1.

2.2. Synthesis. The SZMF catalysts were prepared using the wet impregnation method, and the details are given in SI Section 2 (Figure S1). The obtained catalysts were marked as SZMFy% (y is the Fe_2O_3 content, wt %). The same procedure was used to prepare SZM without the $Fe(NO_3)_3$ precursor, and the catalysts with the ZrO_2/MCM-41 weight ratio of 1/2, 1/1, and 2/1 were named as SZM1/2, SZM1/1, and SZM2/1.

2.3. Characterization. The studied catalysts were characterized by X-ray diffraction (XRD), Fourier transform infrared spectroscopy (FT-IR), scanning electron microscopy (SEM), transmission electron microscopy (TEM), X-ray photoelectron spectroscopy (XPS), inductively coupled plasma optical emission spectroscopy (ICP-OES), N_2 adsorption/desorption experiment, ultraviolet−visible spectroscopy (UV−vis), pyridine-adsorption infrared spectroscopy (Py-IR), and temperature programed desorption of ammonia/CO_2 (NH_3/CO_2-TPD). The details about these methods are listed in SI Section 3.

DOI: 10.1021/acs.est.9b01901
Environ. Sci. Technol. 2019, 53, 6094−6102

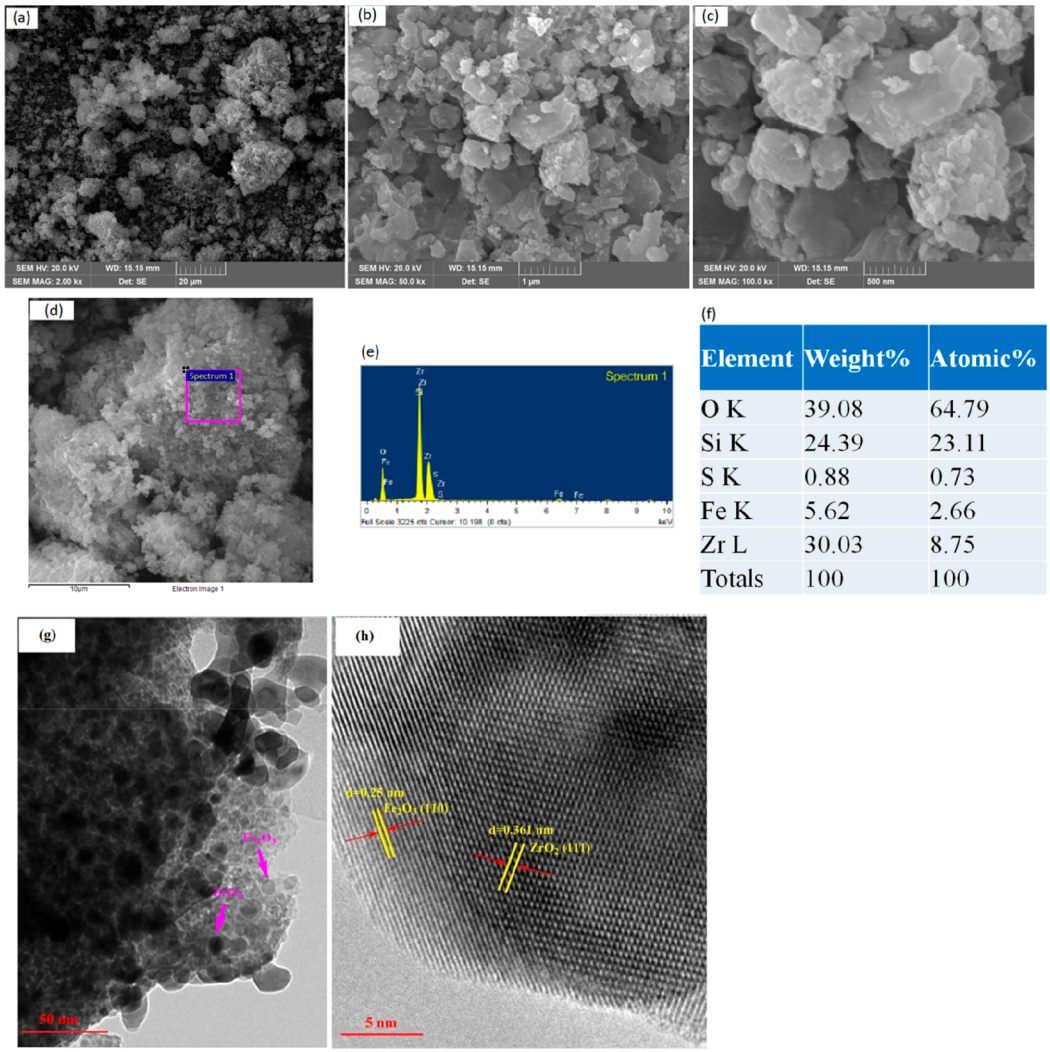

Element	Weight%	Atomic%
O K	39.08	64.79
Si K	24.39	23.11
S K	0.88	0.73
Fe K	5.62	2.66
Zr L	30.03	8.75
Totals	100	100

Figure 2. (a)-(c) SEM image of SZMF10%, (d) the SEM image from which the presented EDX measurement was acquired, (e) SEM-EDX spectrum, (f) the mass fraction of the catalyst, and (g) and (h) TEM and HRTEM images of SZMF10%.

2.4. Catalytic Desorption Test. The catalytic CO_2 desorption test was conducted based on the method reported by Zhang et al.,[49] and the details about this test are available in SI Section 4 (Figure S2(a)). The reliability analysis of experimental data is presented in SI Section 4 (Table S1).

2.5. CO_2 Absorption Experiment. The CO_2 absorption behavior of the catalytically desorbed MEA solution was studied using a batch-type CO_2 absorption setup reported by Gao et al.,[50] and the details about this absorption test are given in SI Section 5 (Figure S2(b)).

2.6. Calculation. Five evaluation parameters, namely, CO_2 desorption rate (DR, mol/min), cyclic capacity (CC, mol), heat duty (HD, kJ/mol), relative heat duty (RH, %), and desorption factor (DF, $mol^3/(kJ{\cdot}min)$), were defined and applied to fully assess the catalytic CO_2 desorption performance of the prepared catalysts. The definitions and calculation equations of the five parameters are available in SI Sections 4 and 6.

3. RESULTS AND DISCUSSION

3.1. Catalytic CO_2 Desorption. The CO_2 desorption curves of rich 5 M MEA solutions with five different catalysts (SZ, MCM-41, SZM1/2, SZM1/1, and SZM2/1) are displayed in Figure 1(a),(b). In the present study, the CO_2 desorption performance was evaluated with regards to the DR, CC, and HD within the first 1.5 h of the CO_2 desorption experiment, and these results are reported in Table S2. The results show that the addition of the five catalysts enhanced CO_2 desorption kinetics over the blank run, and three SZM catalysts display superior catalytic activity than that of the single catalysts. The SZM1/1 presents the best catalytic performance, which lowered the heat duty by 24.6% and increased the desorption factor by about 116% compared with the blank test. It is noteworthy that the lean CO_2 loading of each MEA system equilibrated at around 0.35 mol CO_2/mol amine, which depends on the final temperature of the desorption process. This indicated that the introduction of the catalyst just facilitated the desorption kinetics but would not alter the reaction equilibrium.

In order to further improve the desorption performance of the SZM1/1 catalyst, a series of Fe_2O_3 modified SZM1/1 (SZMF) catalysts (i.e., SZMF5%, SZMF10%, and SZMF15%) were prepared and used for the CO_2 desorption process. Figure 1(c) shows the catalytic CO_2 desorption performances of MEA with three SZMF catalysts. Note that three SZMF catalysts can further improve the desorption kinetics compared to the SZM1/1. Among three catalysts, SZMF10% presents the

DOI: 10.1021/acs.est.9b01901
Environ. Sci. Technol. 2019, 53, 6094−6102

best catalytic activity, followed by SZMF5%, and then SZMF15%. Likewise, the lean CO_2 loading of each MEA-catalyst system reached equilibrium with about 0.35 mol CO_2/mol amine.

The DR, CC, and HD for these systems within the first 1.5 h are summarized in Table S2. With the introduction of the SZMF10%, the desorption rate of MEA respectively accelerated by 19.3% and 51.8% in comparison with the use of SZM1/1 and the blank run. Compared to the catalyst-free test, the addition of SZMF catalysts increased the cyclic capacity by 38.1−54.7%. As shown in Figure 1(d), with the presence of SZMF catalysts, the relative heat duty (%) followed the order of SZMF10% (60.6) < SZMF5% (66.0) < SZMF15% (72.3) < SZM1/1 (75.4) < blank (100.0). Markedly, the use of SZMF catalysts improved the desorption factor by 260−388% in comparison with the catalyst-free run (Figure 1(e)). Accordingly, the SZMF catalysts further improved the CO_2 desorption performance with regards to the higher desorption rate, bigger cyclic capacity, and lower heat duty. The higher CO_2 desorption kinetics signifies that the lower reboiler temperature (i.e., lower heat duty) was required with the introduction of the catalyst to strip the same amount of CO_2 by comparing with the blank run. Additionally, the same cyclic CO_2 capacity (mol/mol) requires a higher flow rate for the amine solution with the addition of the catalyst at the fixed reboiler temperature by comparing with that of the blank run, leading to a low energy consumption (kJ/kg CO_2).[51,52]

The comparison of the catalytic performances for the SZMF catalysts at different CO_2 desorption times (i.e., 1, 1.5, and 2 h) is presented in SI Figure S4. Note that the catalytic desorption performance shows the similar change trends at different times. Table S3 lists the comparisons of catalytic rich MEA solution regeneration performances of various reported catalysts. Note that the SZMF10% shows the best catalytic CO_2 desorption performance compared to the reported catalysts including single zeolites, metal oxides, carbonic anhydrase, and metal modified zeolites. However, the investigation of the CO_2 capture performance of the novel and/or blended amine systems with the SZMF catalyst is essential to further advance this catalyst-mediated CO_2 capture technology in the future.

3.2. Catalyst Characteristics. *3.2.1. XRD, FT-IR, and ICP Test.* The XRD patterns of SZMF10%, MCM-41, SZ, and Fe_2O_3 and FT-IR spectra of SZ, MCM-41, SZMF5%, SZMF10%, and SZMF15% are shown in Figure S5. XRD patterns and IR spectra indicated that the iron and zirconium species were successfully dispersed on the surface of MCM-41, the metal atoms and SO_4^{2-} were incorporated into the framework of MCM-41, and the main mesoporous structure of MCM is preserved (SI Section 8.1). The actual metal loadings (Zr, Fe) of SZMF catalysts were obtained by the ICP tests (Table S4). Note that the actual metal oxide loadings of the SZMF catalysts present the reasonable experimental error compared to the normal value.

3.2.2. TEM and SEM. The SEM results of the SZMF10% are displayed in Figure 2. Note that the bright small particle of the surface is associated with Fe_2O_3, while the sombrous large aggregated particle is attributed to ZrO_2. Also, some small particles of Fe_2O_3 may be dispersed on large particles of ZrO_2. Figure 2(e),(f) displays the EDX data of SZMF10%, which implies that this catalyst contains the elemental constituents of S, Zr, and Fe as expected and the successful support of the SO_4^{2-}/ZrO_2 and Fe_2O_3. Note that the Fe and Zr contents are 5.62 and 30.03 wt %, respectively, which show the approximate experimental error in comparison with the ICP results (6.63 and 33.2%, Table S4). These results further verify that the SZMF10% catalyst was successfully synthesized.

Figure 2(g),(h) shows the TEM and HRTEM images of SZMF10%. Note that this catalyst displays the ordered arrays, implying that the main silica structure of MCM-41 is retained after supporting the Fe_2O_3 and SO_4^{2-}/ZrO_2. The plentiful Fe_2O_3 and ZrO_2 particles are aggregated together and formed local accumulation (oval). The HRTEM image presents the lattice fringe spacing of 0.25 nm corresponding to the (110) plane of Fe_2O_3,[53] while the lattice fringe spacing of 0.361 nm corresponds to the (111) plane of ZrO_2,[54] which is in well accordance with the results of XRD (Figure 2(h)). The results further indicated that the Fe and Zr species were well dispersed on the surface of the support MCM-41. Moreover, the lattice fringes of Fe_2O_3 and ZrO_2 are cross-linked with each other, implying that there might be strong structure-interaction between the two metal oxides in the SZMF10%,[55,56] which further confirms the results of FT-IR.

3.2.3. Textural Properties of Catalysts. The N_2 desorption isotherms of SZ, MCM-41, and SZMF are shown in Figure S5(d), and structural properties of these catalysts are tabulated in Table S5. All the catalysts presented similar type IV isotherms, which are typical characteristics of the mesoporous structure. The pore size distributions of the SZMF further verified that the catalysts mainly possess the mesoporous structure (Figure S6). The surface area of MCM-41 is 1058.6 m^2/g, while it reduced significantly from 382.5 to 458.7 m^2/g for the SZMF catalysts. After the insertion of SZ and Fe into the MCM-41, a drastic reduction in the BET surface area (56.7−63.9% lower) and pore volume (48.8−70.7% lower) is observed.

Interesting, the surface area and pore volume of SZMF are increased with the increase of the contents of Fe_2O_3. This can be attributed to the Fe_2O_3 interacting with MCM-41 or ZrO_2 producing a new complex structure, which assists in impeding the particle growth of metal oxides, and thus leading to the higher surface area and pore volume. This is well consistent with the results of FT-IR and SEM and the results of previous work.[57,58] Due to these catalysts are the mesoporous structures, and the BET surface areas mainly belong to the mesoporous surface areas. Commonly, the large mesoporous structure (>4 nm) has the main effect on the diffusion of reactants and products. Thus, the variation in the pore size may play a favorable role in catalytic CO_2 desorption performances.

3.2.4. XPS and UV−vis. The XPS analysis results of SZMF10% are shown in Figure S7. The results suggested that Fe species were primarily in trivalent status Fe(III) in the oxide and that the Zr species were mainly in Zr(IV) in the oxide. The XPS results also proved that the metal species highly dispersed on the surface of mesoporous support MCM-41, which may lead to the superior catalytic CO_2 desorption performance of SZMF (SI Section 8.2).

UV−vis spectra of SZMF catalysts were obtained and used to study the chemical environment and nature of Fe species in the framework of support MCM-41. Compared with the two other catalysts, the spectrum indicated that SZMF10% has a higher content of isolated Fe^{3+} cations (tetrahedrally coordinated Fe), which may result in the higher catalytic CO_2 desorption performance (SI Section 8.3, Figure S8(a)).

DOI: 10.1021/acs.est.9b01901
Environ. Sci. Technol. 2019, 53, 6094−6102

3.2.5. Surface Acidity and Basicity. The acid types (BAS and LAS) of catalysts were determined by Py-IR, and the results are reported in Figure S8(b) and Table S5. Note that the SZMF catalysts present enhanced BAS and the B/L ratio compared with the MCM-41 and SZ, while the LAS of SZMF were decreased. The B/L ratio of these catalysts decreased in the following order: SZMF10% > SZMF5% > SZMF15% ≫ MCM-41 > SZ. This order is consistent with the catalytic performance of these catalysts. The possible structural framework of SZMF and two ways to form the BAS and LAS are displayed in Figure S9. The acid concentrations of SZMF catalysts were detected using NH_3-TPD. Note that the SZMF10% shows the predominant weak acid sites (110 and 226 °C), and the SZMF5% and SZMF15% almost do not display weak acid sites. The dominant weak acid sites of SZMF10% might be related to their superior catalytic CO_2 desorption (Figure S8(c), SI Section 8.4).

The CO_2-TPD was used to determine the basicity of SZMF10%. The TPD profile (Figure S8(d)) suggests that SZMF10% possesses the weak, medium, and strong basic sites. The probable formation mechanism of basic sites on the SZMF catalyst is displayed in Figure S9(b). The enhanced basic sites of SZMF10% may also lead to its excellent catalytic CO_2 desorption performance compared with the MCM-41 (SI Section 8.5).

3.3. Catalytic Mechanism and Structure−Activity Relationship. *3.3.1. Analysis of Catalytic Mechanism.* The rich MEA solution regeneration process could be explained by the zwitterion mechanism.[59] This mechanism involves two steps, namely: (a) $MEACOO^-$ (carbamate) breakdown and (b) $MEAH^+$ (protonated amine) deprotonation. The difficulty of transfer of proton from $MEAH^+$ to neutral water and strongly endothermic reaction of $MEACOO^-$ breakdown contribute to the high energy demanded for the CO_2-loaded MEA solution regeneration process.[29,30] Earlier work reported that the HCO_3^- groups could behave as catalyst for reaction 3 and decrease the energy barrier of proton transfer. However, there is only a small amount of HCO_3^- groups generated at a higher CO_2 loading region in the MEA solution.[27] Accordingly, there are two promising ways to promote CO_2 desorption at the lower temperature. One is providing the abundant protons to take part in reaction 1, and the other is offering the accessible basic medium (the imitation role of HCO_3^-) to participate in reactions 2 and 3.

(a) $MEACOO^-$ breakdown

$$MEACOO^- + H_3O^+ \leftarrow\rightarrow \text{Zwitterion} \leftarrow\rightarrow MEA + CO_2\uparrow \quad (1)$$

(b) $MEAH^+$ deprotonation

$$MEAH^+ + H_2O \leftarrow\rightarrow MEA + H_3O^+ \quad (2)$$

$$MEAH^+ + HCO_3^- \leftarrow\rightarrow MEA + H_2CO_3 \quad (3)$$

As mentioned above, the SZMF simultaneously possess the favorable acid and basic sites. Based on the zwitterion mechanism, we proposed a dual sites catalytic CO_2 desorption mechanism over the SZMF catalyst. The basic sites imitate the role of HCO_3^- and take part in the $MEAH^+$ deprotonation reaction, while the acid sites attend firsthand the MEA-COO^- dissociation reaction. The possible catalytic reaction pathway is depicted in Figure 3.

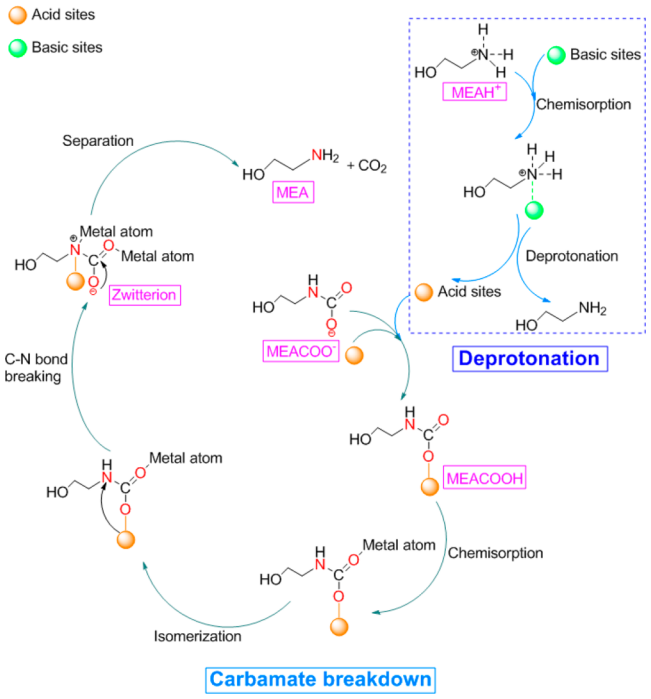

Figure 3. A possible catalytic CO_2 desorption mechanism over the SZMF catalyst.

The catalytic desorption process was briefly described as follows.[60] As shown in the upper-right corner of Figure 3, after the addition of the SZMF catalyst, the basic sites will join in the deprotonation reaction and carry off the protons from the $MEAH^+$ to MEA-COO^-. For the MEA-COO^- breakdown reaction, the acid sites which from the deprotonation reaction or the SZMF catalyst will react with MEA-COO^- and transform into MEA-COOH. Afterward, the metal atoms (Fe, Zr) attack the O atom, and then the chemisorption process occurs between the O atom and metal atoms. Third, there is an isomerization process where the acid sites shift from the O to the N atoms. Fourthly, the acid sites rob the lone pair of electrons of the N atom, the configuration of the N atom will be transferred from sp^2 to sp^3, and after that the strength of the C−N bond will be weakened by stretching. Moreover, the metal atoms will further assault the N atom and aid to stretch the C−N bond for enhancing CO_2 desorption performance. At last, the C−N bond is destroyed, and the zwitterion divides into MEA and CO_2.

Regarding the recovery of the spent catalyst, which supplements it with or restores its protons, it is achieved via the $MEAH^+$ deprotonation reaction which supplies protons back up to the spent catalyst from the MEA. Evidently, when the MEA system has the SZMF catalyst, the additional molecular force is provided by the chemical bond to attenuate the C−N bond, which leads to a significant reduction of the activation energy and the faster CO_2 desorption at lower temperature. In other words, part of the theoretical energy demanded for CO_2 desorption is offered up by the catalyst in the forms of proton donation or acceptance (offered chemical energy) and therefore decreasing the energy needed (i.e., external energy) for CO_2 desorption.

3.3.2. Elaboration of Structure−Activity Relationship. Several properties of the catalyst may influence the catalytic desorption activity including, acid sites, basic sites, the B/L ratio, and surface area. Liang et al.[24] disclosed that MSA and

DOI: 10.1021/acs.est.9b01901
Environ. Sci. Technol. 2019, 53, 6094−6102

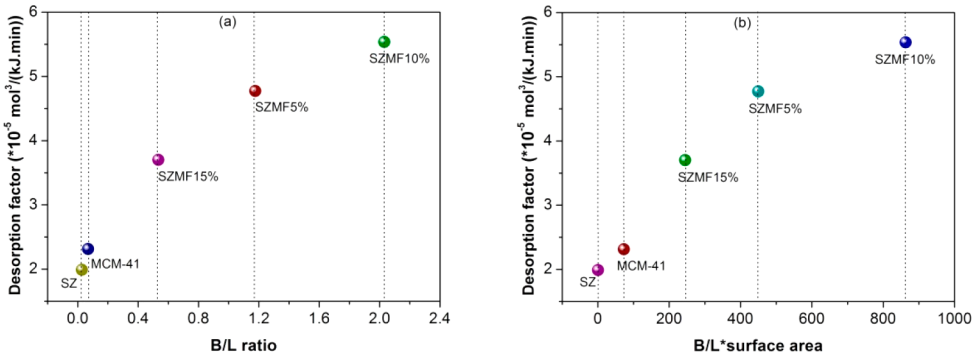

Figure 4. Relationship between the desorption factor and the properties of catalyst: (a) the B/L ratio and (b) the product of the B/L ratio and surface area.

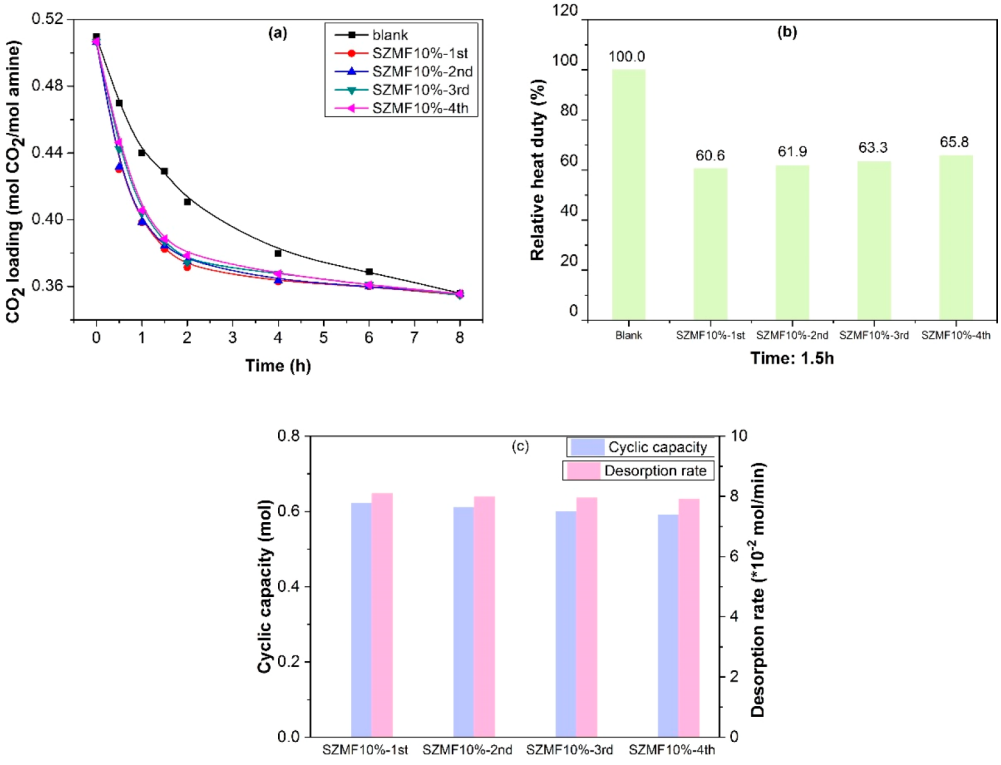

Figure 5. Recyclability test of the SZMF10%: (a) loading change curves, (b) relative heat duty, and (c) CO_2 desorption rate and cyclic capacity.

the B/L ratio of the catalyst had a favorable effect on the catalytic activity. The relations between the catalytic behaviors in terms of DF and properties were investigated for MEA solution with SZMF catalysts. As shown in Figure 4(a), the DF was almost linearly related to the B/L ratio, and the catalytic activities increased with an increase in the value of the B/L ratio. A similar trend was observed in Figure 4(b) for the product of the B/L ratio and surface area (B/L*surface area). These results are in good agreement with previous work[10] and further demonstrated that the B/L ratio and B/L*surface area play the predominant role on the catalytic CO_2 desorption activity.

NH_3-TPD results show that the SZMF10% possesses the higher weak acid sites than the other two SZMF catalysts, thus the weak acid sites may have a positive effect on the catalytic performance. Besides, combining the result of CO_2-TPD and catalytic mechanism analysis, it is concluded that the basic sites are beneficial for the catalytic regeneration process. Based on the results of UV−vis spectra, the higher content of isolated Fe^{3+} species is also responsible for the superior catalytic CO_2 desorption activity of SZMF. These results demonstrated that the B/L ratio, B/L*surface area, weak acid sites, basic sites, and high content of isolated Fe^{3+} species are to the benefit of the solvent regeneration process, and the B/L*surface area and basic sites play a key role in enhancing their catalytic activity.

3.4. Stability of the Catalyst. The cyclic stability of the SZMF10% catalyst was studied for four cycles under the same desorption conditions. After the regeneration experiment was completed, the used SZMF catalyst was recycled by washing, vacuum filtration (vacuum pump: SHB-III, pumping capacity: 10 L/min; filter paper pore size of 1−3 μm), and drying in the drying oven (DHG-9070A) at 110 °C for 10 h and then used for the next cycle. The results after four cycles of testing for SZMF10% are reported in Figure 5. As shown in Figure 5(a), (c), the desorption rate and cyclic capacity have almost no change after four cyclic tests. For the heat duty, after four times usage of SZMF10%, about 92% of the catalytic activity still maintained when compared to the fresh catalyst (Figure 5(b)).

DOI: 10.1021/acs.est.9b01901
Environ. Sci. Technol. 2019, 53, 6094−6102

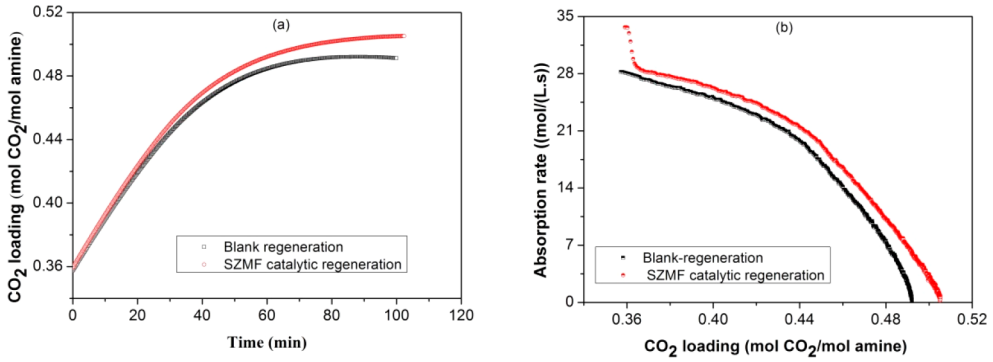

Figure 6. CO_2 absorption performance of the regenerated MEA solution: (a) loading change curves and (b) absorption rate curves.

Consequently, these results indicate that SZMF10% possesses an excellent recyclability. The FT-IR spectrum and XRD pattern of the spent catalyst further confirm that the structure of the catalyst was retained after the fourth cyclic test (Figure S10). Therefore, the decrease of the catalytic activity of SZMF10% may be related to the loss of the powder of catalyst during the stability run. Nevertheless, the investigation of recyclability of the SZMF catalyst in the catalytic CO_2 desorber for many cycles is demanded in the future.

3.5. Effect of CO_2 Absorption Performance. The investigation on the CO_2 absorption behavior of the catalytically regenerated MEA solution was conducted in this work. As shown in Figure 6, the catalytically regenerated MEA solution shows superior CO_2 absorption performance than that of blank regenerated MEA solution. The enhanced absorption performance might be attributed to the formation of metal-amine complexation, which improves the CO_2 absorption activity and absorption capacity. This is in well accord with the results of a study by Yu et al.[19,21] Their study revealed that the addition of Cu(II)/Ni(II) ion into MEA solution improved the CO_2 absorption performance by generating the Cu/Ni-MEA complexes. However, further study is required to identify the species formed in this system to fully understand this enhanced absorption mechanism in the future.

■ ASSOCIATED CONTENT

Supporting Information

The Supporting Information is available free of charge on the ACS Publications website at DOI: 10.1021/acs.est.9b01901.

Lists of chemicals; synthesis of catalysts (Figure S1); CO_2 desorption/absorption experiment (Figure S2); CO_2 loading titration apparatus (Figure S3); catalyst characterization techniques and results (XRD, FT-IR, ICP, BET, XPS, UV−vis, NH_3/CO_2-TPD; Figures S5−S8, S10; Tables S4, S5); analysis for reliability of experimental data (Table S1), comparison of catalytic desorption performance for different catalysts-MEA systems at different regeneration times (Figure S4); catalytic CO_2 desorption performance of SZM and SZMF catalysts (Table S2); comparisons of catalytic CO_2 desorption of different reported catalysts (Table S3) (PDF)

■ AUTHOR INFORMATION

Corresponding Authors

*E-mail: hxgao@hnu.edu.cn (H.G.).
*E-mail: zwliang@hnu.edu.cn (Z.L.).

ORCID

Zhiwu Liang: 0000-0003-1935-0759

Notes

The authors declare no competing financial interest.

■ ACKNOWLEDGMENTS

The authors are thankful for the financial support from the National Natural Science Foundation of China (NSFC-Nos. 21536003, 21706057, 21606078, 51521006, 21776065, and 21808049), the Natural Science Foundation of Hunan Province in China (No. 2018JJ3033), the China Outstanding Engineer Training Plan for Students of Chemical Engineering & Technology in Hunan University (MOE-No. 2011-40), the China Scholarship Council (201806130065), and the Hunan Provincial Innovation Foundation for Postgraduate (CX2018B154).

■ REFERENCES

(1) Liang, Z. H.; Rongwong, W.; Liu, H.; Fu, K.; Gao, H.; Cao, F.; Zhang, R.; Sema, T.; Henni, A.; Sumon, K. Recent progress and new developments in post-combustion carbon-capture technology with amine based solvents. *Int. J. Greenhouse Gas Control* **2015**, *40*, 26−54.
(2) Zhang, S.; Du, M.; Shao, P.; Wang, L.; Ye, J.; Chen, J.; Chen, J. Carbonic anhydrase enzyme-MOFs composite with a superior catalytic performance to promote CO_2 absorption into tertiary amine solution. *Environ. Sci. Technol.* **2018**, *52* (21), 12708−12716.
(3) Zhang, S.; Shen, Y.; Shao, P.; Chen, J.; Wang, L. Kinetics, thermodynamics, and mechanism of a novel biphasic solvent for CO_2 capture from flue gas. *Environ. Sci. Technol.* **2018**, *52* (6), 3660−3668.
(4) Chandan, P. A.; Remias, J. E.; Neathery, J. K.; Liu, K. Morpholine nitrosation to better understand potential solvent based CO_2 capture process reactions. *Environ. Sci. Technol.* **2013**, *47* (10), 5481−5487.
(5) Lai, Q.; Diao, Z.; Kong, L.; Adidharma, H.; Fan, M. Amine-impregnated silicic acid composite as an efficient adsorbent for CO_2 capture. *Appl. Energy* **2018**, *223*, 293−301.
(6) Zhang, S.; Lu, Y. Surfactants facilitating carbonic anhydrase enzyme-mediated CO_2 absorption into a carbonate solution. *Environ. Sci. Technol.* **2017**, *51* (15), 8537−8543.
(7) Li, Q.; Wang, Y.; An, S.; Wang, L. Kinetics of CO_2 absorption in concentrated K2CO3/PZ mixture using a wetted-wall column. *Energy Fuels* **2016**, *30* (9), 7496−7502.
(8) Xu, X.; Wood, C. D. A Highly Tunable Approach to Enhance CO_2 Capture with Liquid Alkali/amines. *Environ. Sci. Technol.* **2018**, *52* (18), 10874−10882.
(9) Jiang, K.; Li, K.; Puxty, G.; Yu, H.; Feron, P. H. Information Derivation from Vapor-Liquid Equilibria Data: A Simple Shortcut to Evaluate the Energy Performance in an Amine-Based Postcombustion CO_2 Capture. *Environ. Sci. Technol.* **2018**, *52* (18), 10893−10901.

DOI: 10.1021/acs.est.9b01901
Environ. Sci. Technol. 2019, 53, 6094−6102

(10) Zhang, X.; Zhang, X.; Liu, H.; Li, W.; Xiao, M.; Gao, H.; Liang, Z. Reduction of energy requirement of CO_2 desorption from a rich CO_2-loaded MEA solution by using solid acid catalysts. *Appl. Energy* **2017**, *202*, 673−684.
(11) Matin, N. S.; Steckel, J. A.; Thompson, J.; Sarma, M.; Liu, K. Application of Surface Tension Model for Prediction of Interfacial Speciation of CO_2-Loaded Aqueous Solutions of Monoethanolamine. *Ind. Eng. Chem. Res.* **2017**, *56* (19), 5747−5755.
(12) Widger, L. R.; Combs, M.; Lohe, A. R.; Lippert, C. A.; Thompson, J. G.; Liu, K. Selective Removal of Nitrosamines from a Model Amine Carbon-Capture Waterwash Using Low-Cost Activated-Carbon Sorbents. *Environ. Sci. Technol.* **2017**, *51* (18), 10913−10922.
(13) Liang, Z.; Fu, K.; Idem, R.; Tontiwachwuthikul, P. Review on current advances, future challenges and consideration issues for post-combustion CO_2 capture using amine-based absorbents. *Chin. J. Chem. Eng.* **2016**, *24* (2), 278−288.
(14) Jiang, K.; Li, K.; Yu, H.; Chen, Z.; Wardhaugh, L.; Feron, P. Advancement of ammonia based post-combustion CO_2 capture using the advanced flash stripper process. *Appl. Energy* **2017**, *202*, 496−506.
(15) Wang, L.; Zhang, Y.; Wang, R.; Li, Q.; Zhang, S.; Li, M.; Liu, J.; Chen, B. Advanced Monoethanolamine Absorption Using Sulfolane as a Phase Splitter for CO_2 Capture. *Environ. Sci. Technol.* **2018**, *52* (24), 14556−14563.
(16) Shao, L.; Li, Y.; Huang, J.; Liu, Y.-N. Synthesis of Triazine-Based Porous Organic Polymers Derived N-Enriched Porous Carbons for CO_2 Capture. *Ind. Eng. Chem. Res.* **2018**, *57* (8), 2856−2865.
(17) Zhang, R.; Zhang, X.; Yang, Q.; Yu, H.; Liang, Z.; Luo, X. Analysis of the reduction of energy cost by using MEA-MDEA-PZ solvent for post-combustion carbon dioxide capture (PCC). *Appl. Energy* **2017**, *205*, 1002−1011.
(18) Lai, Q.; Toan, S.; Assiri, M. A.; Cheng, H.; Russell, A. G.; Adidharma, H.; Radosz, M.; Fan, M. Catalyst-TiO $(OH)_2$ could drastically reduce the energy consumption of CO_2 capture. *Nat. Commun.* **2018**, *9* (1), 2672.
(19) Li, K.; van der Poel, P.; Conway, W.; Jiang, K.; Puxty, G.; Yu, H.; Feron, P. Mechanism investigation of advanced metal-ion-mediated amine regeneration: a novel pathway to reducing CO_2 reaction enthalpy in amine-based CO_2 capture. *Environ. Sci. Technol.* **2018**, *52* (24), 14538−14546.
(20) Yu, B.; Yu, H.; Li, K.; Ji, L.; Yang, Q.; Wang, X.; Chen, Z.; Megharaj, M. A Diamine-Based Integrated Absorption-Mineralization Process for Carbon Capture and Sequestration: Energy Savings, Fast Kinetics, and High Stability. *Environ. Sci. Technol.* **2018**, *52* (22), 13629−13637.
(21) Cheng, C. H.; Li, K.; Yu, H.; Jiang, K.; Chen, J.; Feron, P. Amine-based post-combustion CO_2 capture mediated by metal ions: Advancement of CO_2 desorption using copper ions. *Appl. Energy* **2018**, *211*, 1030−1038.
(22) Shao, L.; Sang, Y.; Huang, J.; Liu, Y.-N. Triazine-based hyper-cross-linked polymers with inorganic-organic hybrid framework derived porous carbons for CO_2 capture. *Chem. Eng. J.* **2018**, *353*, 1−14.
(23) Legrand, L.; Schaetzle, O.; de Kler, R.; Hamelers, H. V. Solvent-Free CO_2 Capture Using Membrane Capacitive Deionization. *Environ. Sci. Technol.* **2018**, *52* (16), 9478−9485.
(24) Liang, Z.; Idem, R.; Tontiwachwuthikul, P.; Yu, F.; Liu, H.; Rongwong, W. Experimental study on the solvent regeneration of a CO_2 loaded MEA solution using single and hybrid solid acid catalysts. *AIChE J.* **2016**, *62* (3), 753−765.
(25) Shi, H.; Naami, A.; Idem, R.; Tontiwachwuthikul, P. Catalytic and non catalytic solvent regeneration during absorption-based CO_2 capture with single and blended reactive amine solvents. *Int. J. Greenhouse Gas Control* **2014**, *26* (7), 39−50.
(26) Srisang, W.; Pouryousefi, F.; Osei, P. A.; Decardi-Nelson, B.; Akachuku, A.; Tontiwachwuthikul, P.; Idem, R. Evaluation of the heat duty of catalyst-aided amine-based post combustion CO_2 capture. *Chem. Eng. Sci.* **2017**, *170*, 48−57.
(27) Liu, H.; Zhang, X.; Gao, H.; Liang, Z.; Idem, R.; Tontiwachwuthikul, P. Investigation of CO_2 regeneration in single and blended amine solvents with and without catalyst. *Ind. Eng. Chem. Res.* **2017**, *56* (27), 7656−7664.
(28) Bhatti, U. H.; Shah, A. K.; Kim, J. N.; You, J. K.; Choi, S. H.; Lim, D. H.; Nam, S.; Park, Y. H.; Baek, I. H. Effects of Transition Metal Oxide Catalysts on MEA Solvent Regeneration for the Post-Combustion Carbon Capture Process. *ACS Sustainable Chem. Eng.* **2017**, *5* (7), 5862−5868.
(29) Zhang, X.; Liu, H.; Liang, Z.; Idem, R.; Tontiwachwuthikul, P.; Al-Marri, M. J.; Benamor, A. Reducing energy consumption of CO_2 desorption in CO_2-loaded aqueous amine solution using Al2O3/HZSM-5 bifunctional catalysts. *Appl. Energy* **2018**, *229*, 562−576.
(30) Zhang, X.; Hong, J.; Liu, H.; Luo, X.; Olson, W.; Tontiwachwuthikul, P.; Liang, Z. SO_4^2/ZrO_2 supported on γ Al_2O_3 as a catalyst for CO_2 desorption from CO_2 loaded monoethanolamine solutions. *AIChE J.* **2018**, *64* (11), 3988−4001.
(31) Wang, T.; Yu, W.; Liu, F.; Fang, M.; Farooq, M.; Luo, Z. Enhanced CO_2 absorption and desorption by monoethanolamine (MEA)-based nanoparticle suspensions. *Ind. Eng. Chem. Res.* **2016**, *55* (28), 7830−7838.
(32) Sahoo, P. C.; Kumar, M.; Singh, A.; Singh, M. P.; Puri, S. K. Biocatalyzed Accelerated Post-combustion CO_2 Capture and Stripping in Monoethanolamine. *Energy Fuels* **2017**, *31* (10), 11007−11012.
(33) Bhatti, U. H.; Nam, S.; Park, S.; Baek, I. H. Performance and mechanism of metal oxide catalyst-aided amine solvent regeneration. *ACS Sustainable Chem. Eng.* **2018**, *6* (9), 12079−12087.
(34) Bhatti, U. H.; Sivanesan, D.; Lim, D. H.; Nam, S. C.; Park, S.; Baek, I. H. Metal oxide catalyst-aided solvent regeneration: A promising method to economize post-combustion CO_2 capture process. *J. Taiwan Inst. Chem. Eng.* **2018**, *93*, 150−157.
(35) Zhang, X.; Huang, Y.; Gao, H.; Luo, X.; Liang, Z.; Tontiwachwuthikul, P. Zeolite catalyst-aided tri-solvent blend amine regeneration: An alternative pathway to reduce the energy consumption in amine-based CO_2 capture process. *Appl. Energy* **2019**, *240*, 827−841.
(36) Zhang, H.; Yu, H.; Zheng, A.; Li, S.; Shen, W.; Deng, F. Reactivity enhancement of 2-propanol photocatalysis on SO_4^2/TiO_2: insights from solid-state NMR spectroscopy. *Environ. Sci. Technol.* **2008**, *42* (14), 5316−5321.
(37) Saravanan, K.; Tyagi, B.; Bajaj, H. C. Nano-crystalline, mesoporous aerogel sulfated zirconia as an efficient catalyst for esterification of stearic acid with methanol. *Appl. Catal., B* **2016**, *192*, 161−170.
(38) Jiménez-Morales, I.; Moreno-Recio, M.; Santamaría-González, J.; Maireles-Torres, P.; Jiménez-López, A. Production of 5-hydroxymethylfurfural from glucose using aluminium doped MCM-41 silica as acid catalyst. *Appl. Catal., B* **2015**, *164*, 70−76.
(39) Jiménez-Morales, I.; Santamaría-González, J.; Maireles-Torres, P.; Jiménez-López, A. Calcined zirconium sulfate supported on MCM-41 silica as acid catalyst for ethanolysis of sunflower oil. *Appl. Catal., B* **2011**, *103* (1), 91−98.
(40) Shevchenko, N.; Zaitsev, V.; Walcarius, A. Bifunctionalized mesoporous silicas for Cr (VI) reduction and concomitant Cr (III) immobilization. *Environ. Sci. Technol.* **2008**, *42* (18), 6922−6928.
(41) Marteel, A. E.; Tack, T. T.; Bektesevic, S.; Davies, J. A.; Mason, M. R.; Abraham, M. A. Hydroformylation of 1-hexene in supercritical carbon dioxide: characterization, activity, and regioselectivity studies. *Environ. Sci. Technol.* **2003**, *37* (23), 5424−5431.
(42) Dündar-Tekkaya, E.; Yürüm, Y. Mesoporous MCM-41 material for hydrogen storage: A short review. *Int. J. Hydrogen Energy* **2016**, *41* (23), 9789−9795.
(43) Ghedini, E.; Signoretto, M.; Pinna, F.; Cerrato, G.; Morterra, C. Gas and liquid phase reactions on MCM-41/SZ catalysts. *Appl. Catal., B* **2006**, *67* (1), 24−33.
(44) Atanga, M. A.; Rezaei, F.; Jawad, A.; Fitch, M.; Rownaghi, A. A. Oxidative dehydrogenation of propane to propylene with carbon dioxide. *Appl. Catal., B* **2018**, *220*, 429−445.

DOI: 10.1021/acs.est.9b01901
Environ. Sci. Technol. 2019, 53, 6094−6102

(45) Shen, S.; Chen, J.; Koodali, R. T.; Hu, Y.; Xiao, Q.; Zhou, J.; Wang, X.; Guo, L. Activation of MCM-41 mesoporous silica by transition-metal incorporation for photocatalytic hydrogen production. *Appl. Catal., B* **2014**, *150−151* (11), 138−146.
(46) Kwong, C.; Chao, C. Y. H.; Hui, K.; Wan, M. Catalytic ozonation of toluene using zeolite and MCM-41 materials. *Environ. Sci. Technol.* **2008**, *42* (22), 8504−8509.
(47) Chen, Y.; Li, C.; Chen, J.; Tang, X. Self-Prevention of Well-Defined-Facet Fe_2O_3/MoO_3 against Deposition of Ammonium Bisulfate in Low-Temperature NH3-SCR. *Environ. Sci. Technol.* **2018**, *52* (20), 11796−11802.
(48) Bing, J.; Hu, C.; Nie, Y.; Yang, M.; Qu, J. Mechanism of catalytic ozonation in Fe_2O_3/Al_2O_3@ SBA-15 aqueous suspension for destruction of ibuprofen. *Environ. Sci. Technol.* **2015**, *49* (3), 1690−1697.
(49) Zhang, X.; Zhang, R.; Liu, H.; Gao, H.; Liang, Z. Evaluating CO_2 desorption performance in CO_2-loaded aqueous tri-solvent blend amines with and without solid acid catalysts. *Appl. Energy* **2018**, *218*, 417−429.
(50) Gao, H.; Liu, S.; Gao, G.; Luo, X.; Liang, Z. Hybrid behavior and mass transfer performance for absorption of CO_2 into aqueous DEEA/PZ solutions in a hollow fiber membrane contactor. *Sep. Purif. Technol.* **2018**, *201*, 291−300.
(51) Xu, B.; Gao, H.; Chen, M.; Liang, Z.; Idem, R. Experimental Study of Regeneration Performance of Aqueous N, N-Diethylethanolamine Solution in a Column Packed with Dixon Ring Random Packing. *Ind. Eng. Chem. Res.* **2016**, *55* (31), 8519−8526.
(52) Luo, X.; Fu, K.; Yang, Z.; Gao, H.; Rongwong, W.; Liang, Z.; Tontiwachwuthikul, P. Experimental studies of reboiler heat duty for CO_2 desorption from triethylenetetramine (TETA) and triethylenetetramine (TETA)+ N-methyldiethanolamine (MDEA). *Ind. Eng. Chem. Res.* **2015**, *54* (34), 8554−8560.
(53) Cheng, X.; Zhang, X.; Su, D.; Wang, Z.; Chang, J.; Ma, C. NO reduction by CO over copper catalyst supported on mixed CeO_2 and Fe_2O_3: Catalyst design and activity test. *Appl. Catal., B* **2018**, *239*, 485−501.
(54) Liu, W.-J.; Zeng, F.-X.; Jiang, H.; Zhang, X.-S.; Li, W.-W. Composite Fe_2O_3 and ZrO_2/Al_2O_3 photocatalyst: preparation, characterization, and studies on the photocatalytic activity and chemical stability. *Chem. Eng. J.* **2012**, *180*, 9−18.
(55) Li, C.; Li, A.; Luo, Z.; Zhang, J.; Chang, X.; Huang, Z.; Wang, T.; Gong, J. Surviving High Temperature Calcination: ZrO_2 Induced Hematite Nanotubes for Photoelectrochemical Water Oxidation. *Angew. Chem., Int. Ed.* **2017**, *56* (15), 4150−4155.
(56) Cho, J. M.; Lee, S. R.; Sun, J.; Tsubaki, N.; Jang, E. J.; Bae, J. W. Highly ordered mesoporous Fe_2O_3-ZrO_2 bimetal oxides for an enhanced CO hydrogenation activity to hydrocarbons with their structural stability. *ACS Catal.* **2017**, *7* (9), 5955−5964.
(57) Wang, J.-H.; Mou, C.-Y. Characterizations of aluminum-promoted sulfated zirconia on mesoporous MCM-41 silica: Butane isomerization. *Microporous Mesoporous Mater.* **2008**, *110* (2−3), 260−270.
(58) Ye, F.; Dong, Z.; Zhang, H. n-Hexane isomerization over copper oxide-promoted sulfated zirconia supported on mesoporous silica. *Catal. Commun.* **2009**, *10* (15), 2056−2059.
(59) Caplow, M. Kinetics of carbamate formation and breakdown. *J. Am. Chem. Soc.* **1968**, *90* (24), 6795−6803.
(60) Idem, R.; Shi, H.; Gelowitz, D.; Tontiwachwuthikul, P. *Catalytic method and apparatus for separating a gas component from an incoming gas stream.* WO patent US123456 A1 2011, 12013821, 2011.

DOI: 10.1021/acs.est.9b01901
Environ. Sci. Technol. 2019, 53, 6094−6102